Rapid Communications

Sensing chiral magnetic noise via quantum impurity relaxometry

Avinash Rustagi,[1,*] Iacopo Bertelli,[2,3] Toeno van der Sar,[2] and Pramey Upadhyaya[1,4,†]

[1]*School of Electrical and Computer Engineering, Purdue University, West Lafayette, Indiana 47907, USA*

[2]*Department of Quantum Nanoscience, Kavli Institute of Nanoscience, Delft University of Technology, Lorentzweg 1, 2628 CJ, Delft, Netherlands*

[3]*Huygens–Kamerlingh Onnes Laboratorium, Leiden University, Niels Bohrweg 2, 2300 RA, Leiden, Netherlands*

[4]*Purdue Quantum Science and Engineering Institute (PQSEI), Purdue University, West Lafayette, Indiana 47907, USA*

(Received 14 September 2020; accepted 23 November 2020; published 4 December 2020)

We present a theory for quantum impurity relaxometry of magnons in thin films, exhibiting quantitative agreement with recent experiments without needing arbitrary scale factors used in theoretical models thus far. Our theory reveals that chiral coupling between prototypical spin$>1/2$ quantum impurities and magnons plays a central role in determining impurity relaxation, which is further corroborated by our experiments on nickel films interfaced with nitrogen-vacancy centers. Along with advancing magnonics and understanding decoherence in hybrid quantum platforms with magnets, the ability of a quantum impurity spin to sense chiral magnetic noise presents an opportunity to probe chiral phenomena in condensed matter.

DOI: 10.1103/PhysRevB.102.220403

I. INTRODUCTION

Magnons—quanta of spin wave excitations—are fundamental to the understanding of the dynamical properties of magnetically ordered materials. This understanding forms the basis for creating next-generation classical and hybrid quantum technologies in magnonics (an emerging field utilizing magnons as information carriers) [1–3], potentially enabling magnon-mediated coherent control [4] and coupling distant quantum spins [5]. In addition, topological qubit platforms typically involve magnetic materials [6] which could introduce an additional source of decoherence. The rapidly growing field of quantum technology involving magnetic materials makes it imperative to understand the decoherence introduced in quantum systems placed in close proximity to magnetic materials. As such, it is critical to develop sensitive probes for studying the dynamical properties of magnetically ordered materials.

Quantum impurity (QI) relaxometry [7,8]—a sensing scheme measuring the relaxation rate of an impurity spin due to its coupling with magnetic noise [9–12]—has recently emerged as a sensitive, local, and noninvasive technique for probing condensed-matter systems including magnetic materials [13–21]. QIs coupled to magnetic thin films form model systems for developing an understanding of decoherence introduced in qubits that are in close proximity to magnetic materials. It is, therefore, important to develop a predictive model for understanding QI relaxometry of thin film magnons.

Chirality plays a central role for coupling magnons in thin films to QIs. On the one hand, spin transitions are only driven efficiently by rotating magnetic fields of the correct handedness. On the other hand, magnons produce magnetic fields with a handedness that depends on their travel direction (i.e., their fields are chiral).

The zero-field splitting (ZFS) present in typical spin$>1/2$ QIs, such as nitrogen-vacancy (NV) centers in diamond [23,24] and silicon-vacancy centers in SiC [25], gives rise to opposite effective built-in fields causing the different electron spin resonance (ESR) transitions to respond to magnetic field of opposite handedness (provided the applied field is smaller than the ZFS) as demonstrated in NV centers [26]. Additionally, counterpropagating magnons with a nonzero wave-vector component transverse to the equilibrium magnetization and finite out-of-plane deviation (e.g., the Damon-Eschbach modes of thin magnetic films [27]) produce counter-rotating magnetic fields with *unequal* amplitudes [28]. This results from the combined effect of bulk $\rho_m \propto -\vec{\nabla}\cdot\vec{m}$ and surface $\sigma_m \propto \vec{m}\cdot\hat{n}$ (where $\hat{n}$ is the surface normal) magnetic charges [cf. Figs. 1(b) and 1(c)]. Consequently, the $m_s = 0 \rightarrow -1$ and $m_s = 0 \rightarrow +1$ transitions of a prototypical spin-1 QI are driven by magnon-generated fields of different magnitudes. Theoretical models used to analyze experiments [13,14,17] by excluding out-of-plane magnetization fluctuations (and thus σ_m) neglect the role of chirality and require arbitrary scale factors of unknown origin to quantitatively fit the experimentally measured relaxation rates for the $m_s = 0 \rightarrow -1$ and $m_s = 0 \rightarrow +1$ transitions.

In this Rapid Communication, by combining the general theoretical framework of quantum relaxometry [12,15] with Landau-Lifshitz-Gilbert (LLG) phenomenology [29] for magnon dynamics in thin magnetic films, we construct a theory for QI relaxometry of magnons which inherently captures the chiral coupling. As central results, we show that our theory (i) results in excellent quantitative agreement with recent experiments without introducing arbitrary scale factors and (ii) predicts crossover between relaxation rate for the $m_s = 0 \rightarrow -1$ and $m_s = 0 \rightarrow +1$ transitions as a function of

*arustag@purdue.edu
†prameyup@purdue.edu

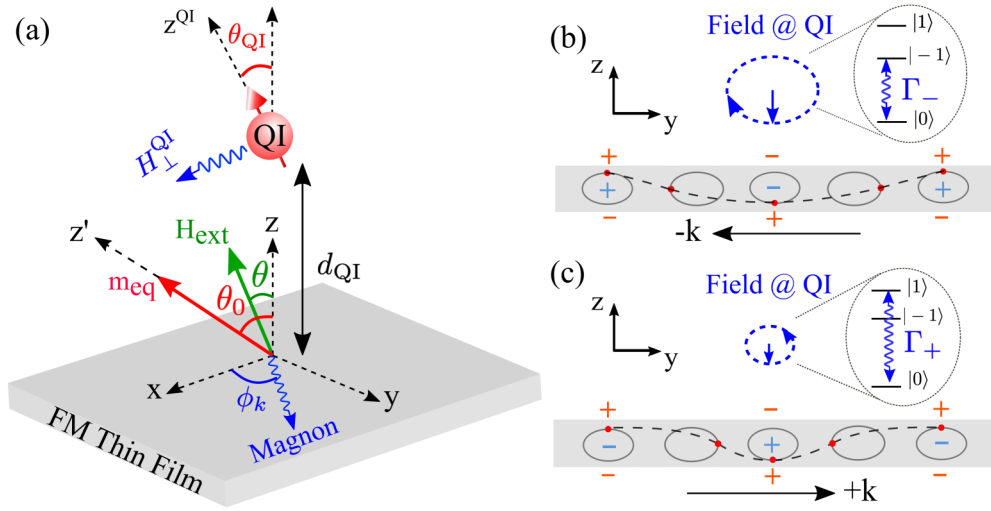

FIG. 1. (a) Schematic of a QI-FM hybrid where the external field is applied along the QI quantization axis ($\theta_{\rm QI} = \theta$) and the direction of equilibrium magnetization is along $\hat{z}'$ (minima of the magnets' free energy). Oppositely handed chiral fields emanating from (b) left- and (c) right-moving magnons couple to (0,−1) and (0,+1) QI transitions, respectively [22]. The effective volume (in light blue color) and surface (in orange color) magnetic charges add (subtract) for left- (right-) moving magnons generating stronger (weaker) dipolar field at the QI.

applied field as an experimental signature of the chiral coupling. We corroborate the latter by presenting data on nickel thin film interfaced with NV-center QI. Our results highlight the importance of chirality in constructing predictive models for advancing magnonics via QI relaxometry. More generally, they suggest that (i) chirality of magnon-generated fields is essential in governing decoherence of quantum systems proximal to magnetic materials and (ii) QI relaxometry can be extended to noninvasively and locally probe the physics of chiral electronic [30–32] and magnetic modes [33,34] living in condensed-matter systems of interest via the magnetic noise emanating from them.

II. RELAXATION MODEL

The hybrid includes a ferromagnetic thin film of thickness L and a QI located at a height $d_{\rm QI}$ above the thin film [cf. Fig. 1(a)]. To evaluate the QI relaxation arising from coupling to the magnetic noise emanating from the film at room temperature, we begin by recasting the relaxation rates of QIs [12,15] in a classical form, relating them to the magnetization correlations.

Here, we consider a prototypical spin-1 QI (like NV center) with spin-triplet ground state $|m_s\rangle$ labeled by the projections $m_s = \{-1, 0, 1\}$ along the QI quantization axis. In the presence of a magnetic field $\vec{H}^{\rm QI}$, the Hamiltonian for the effective two-level systems formed by the states $(|+1\rangle, |0\rangle)$ and $(|0\rangle, |-1\rangle)$ denoted by ξ_+ and ξ_-, respectively, can be written in terms of identity $\mathcal{I}$ and Pauli $\vec{\sigma}$ matrices as

$$\mathcal{H}_{\rm TLS}^{\xi_\pm} = \frac{\omega_\pm^{\rm QI}}{2}[\mathcal{I} \pm \sigma_z] + \frac{\gamma}{2\sqrt{2}}[H_+^{\rm QI}\sigma_- + H_-^{\rm QI}\sigma_+], \quad (1)$$

where γ is the gyromagnetic ratio, $\omega_\pm^{\rm QI} = \Delta \pm \gamma H_z^{\rm QI}$ are the QI-ESR frequencies with the ZFS Δ, and $H_\pm^{\rm QI} = H_x^{\rm QI} \pm iH_y^{\rm QI}$ [35]. The superscript QI denotes that the field components are evaluated in the QI frame (where the z axis is aligned along $z^{\rm QI}$) attained via the rotation matrix $R_{yz}(\theta_{\rm QI}, \phi_{\rm QI})$ (representing rotation about the z axis by $\phi_{\rm QI}$ followed by a rotation about the y axis by $\theta_{\rm QI}$). This form of the Hamiltonian confirms that $m_s = 0 \to -1$ and $m_s = 0 \to +1$ transitions are caused by fields of opposite handedness $H_+^{\rm QI}$ and $H_-^{\rm QI}$, respectively.

The rates corresponding to the transitions $|0\rangle \to |\mp 1\rangle$ (marked by subscript $\mp$) are given by the spectral density of the field perpendicular to the quantization axis evaluated at the ESR frequencies $\omega_\mp^{\rm QI}$ [12,15]: $\Gamma_\mp(\omega_\mp^{\rm QI}) = (\gamma^2/2)\int dt\, e^{i\omega_\mp^{\rm QI} t}\langle H_\pm^{\rm QI}(t)\, H_\mp^{\rm QI}(0)\rangle$ [35]. Here, $\langle ...\rangle$ denotes averaging over the noise realizations.

The Fourier component of the field at QI, due to a spin-wave mode of the film (with an amplitude $\delta\vec{m}'(\vec{k})$, frequency ω, and wave vector $\vec{k}$ which in polar coordinates depends on magnitude k and angle ϕ_k) can be written as $\vec{H}^{\rm QI}(\vec{k}) = \mathcal{D}^{\rm eff}(\vec{k})\delta\vec{m}'(\vec{k})$ [35]. Here, $\delta\vec{m}'(\vec{k})$ is the magnetization deviation in the frame where the z axis is aligned along magnet equilibrium (magnet frame) and $\mathcal{D}^{\rm eff}(\vec{k}) = R_{yz}(\theta_{\rm QI}, \phi_{\rm QI})\mathcal{D}(\vec{k})R_y^T(\theta_0)$ is the rotated dipolar tensor, given

$$\mathcal{D}(\vec{k}) = -2\pi A_k \begin{pmatrix} \cos^2\phi_k & \sin 2\phi_k/2 & i\cos\phi_k \\ \sin 2\phi_k/2 & \sin^2\phi_k & i\sin\phi_k \\ i\cos\phi_k & i\sin\phi_k & -1 \end{pmatrix}, \quad (2)$$

with $A_k = M_s\, e^{-kd_{\rm QI}}[1 - e^{-kL}]$ [36]. Typically, $H_{\rm ext}$ is aligned with the QI axis [see Fig. 1(a)], thus $\theta_{\rm QI} = \theta$ and we choose $\phi_{\rm QI} = 0$ [37].

Substituting the fields from spin waves into the relaxation rate equation of QI, we get

$$\Gamma_\mp(\omega_\mp^{\rm QI}) = \frac{\gamma^2}{2}\int \frac{d\vec{k}}{(2\pi)^2}\sum_{i,j\in\{x,y\}} \mathcal{D}_{\pm i}^{\rm eff}(\vec{k})\mathcal{D}_{\mp j}^{\rm eff}(-\vec{k})C_{ij}(\vec{k}, \omega_\mp^{\rm QI}), \quad (3)$$

where the dipolar tensor elements $\mathcal{D}_{\pm\nu}^{\rm eff} = \mathcal{D}_{x\nu}^{\rm eff} \pm i\mathcal{D}_{y\nu}^{\rm eff}$ (with $\nu = \{x, y\}$), and the correlations between the magnetization

deviations $C_{ij}(\vec{k},\omega)$ is the Fourier transform of $C_{ij}(\vec{r}-\vec{r}\,',t-t') = \langle \delta m_i'(\vec{r},t)\delta m_j'(\vec{r}\,',t')\rangle$ [35]. Equation (3) relates the QI relaxation to the magnetization correlations, which we evaluate next for thermal equilibrium magnons.

III. MAGNON CORRELATIONS

The magnetization (with unit vector $\vec{m}$ and saturation magnetization M_s) dynamics is governed by the LLG equation $\dot{\vec{m}} = -\gamma\,\vec{m}\times[-\partial_{\vec{m}}(\mathcal{F}/M_s)+\vec{h}] + \alpha\,\vec{m}\times\dot{\vec{m}}$, where α is the Gilbert damping and $\vec{h}$ is the excitation field. Here, the free-energy density describing the ferromagnetic thin film includes the Zeeman, exchange, and dipole-dipole energy terms and is given by $\mathcal{F} = -M_s(\vec{H}_{\rm ext}+\vec{H}_D/2)\cdot\vec{m} + M_s(H_{\rm ex}/2)\sum_{i\in\{x,y\}}(\partial_i\vec{m})^2$ where $\vec{H}_{\rm ext}$, $H_{\rm ex}$, and $\vec{H}_D$ are the external, exchange, and demagnetization fields [38]. We find the Fourier domain magnetic susceptibility in response to $\vec{h}'$ (in the magnet frame) by solving the linearized LLG giving $\delta m_i'(\vec{k},\omega) = S_{ij}(\vec{k},\omega)h_j'(\vec{k},\omega)$. The susceptibility matrix is given by

$$S(\vec{k},\omega) = \frac{\gamma}{\Lambda}\begin{pmatrix}\omega_3 - i\alpha\omega & -\omega_1 - i\omega\\ -\omega_1 + i\omega & \omega_2 - i\alpha\omega\end{pmatrix}, \tag{4}$$

where $\omega_0 = \gamma[H_{\rm ext}\cos(\theta_0-\theta) - H_d\cos^2\theta_0 + H_{\rm ex}k^2]$,

$$\begin{aligned}\omega_1 &= \gamma H_d \sin\phi_k\cos\phi_k\cos\theta_0 f_k,\\ \omega_2 &= \omega_0 + \gamma H_d[f_k\cos^2\phi_k\cos^2\theta_0 + (1-f_k)\sin^2\theta_0],\\ \omega_3 &= \omega_0 + \gamma H_d f_k\sin^2\phi_k,\\ \Lambda &= (\omega_2 - i\alpha\omega)(\omega_3 - i\alpha\omega) - \omega_1^2 - \omega^2,\end{aligned} \tag{5}$$

with $H_d = 4\pi M_s$ and $f_k = 1-(1-\exp(-kL))/(kL)$ [35].

In thermal equilibrium, $\vec{h}'$ is the thermal stochastic field with zero mean and local, instantaneous correlation [39,40] $\langle h_i'(\vec{r},t)\,h_j'(\vec{r}\,',t')\rangle = 2D_{th}\delta_{ij}\delta(t-t')\delta(\vec{r}-\vec{r}\,')$ where $D_{th} = \alpha k_B T/(\gamma M_s L)$. Using these stochastic field correlations and the susceptibility matrix elements in Eq. (4), we determine the magnetization correlations:

$$C_{ij}(\vec{k},\omega) = 2D_{\rm th}\sum_{\nu=\{x,y\}} S_{i\nu}(\vec{k},\omega)S_{j\nu}(-\vec{k},-\omega). \tag{6}$$

Equations (3) and (6) are the central theoretical results of our work, describing the impact of thin film magnetization dynamics on the QI-spin relaxation. Particularly, Eq. (6) highlights that all the correlators C_{xx}, C_{xy}, C_{yx}, and C_{yy} are finite. This amounts to including both out-of-plane and in-plane magnetization deviations arising from finite ellipticity of magnons, thereby including the effect of both surface and bulk magnetic charges. Our theory thus inherently captures the chiral nature of magnon noise resulting from the combination of surface and bulk magnetic charges [cf. Figs. 1(b) and 1(c)], and its impact on relaxation via Eq. (3). We thus refer to our theory as chiral theory in the following. Taking the limit where only the in-plane magnetization deviations are included (equivalent to setting $C_{xx} = C_{xy} = C_{yx} = 0$) and modeling the nonzero correlation (C_{yy}) by a Lorentzian, Eqs. (3) and (6) reduce to the existing theoretical models used in Refs. [13,14,17]. Since such models neglect surface charges, the chiral nature of the magnon noise is neglected and we refer to them as the achiral theory.

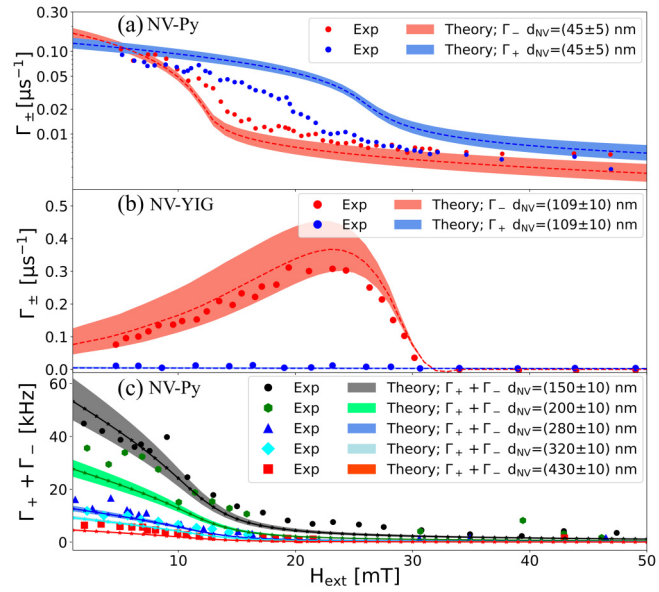

FIG. 2. Comparison of rates evaluated using Eq. (3) to the experimental measurements in hybrids of NV center: (a) Py ($L = 30$ nm, $M_s = 800$ emu/cc, $A_{\rm ex} = 10^{-6}$ erg/cm, $\alpha = 0.015$, $\theta = 36^\circ$) [13], (b) YIG ($L = 20$ nm, $M_s = 124$ emu/cc, $A_{\rm ex} = 3.7\times10^{-7}$ erg/cm, $\alpha = 0.0001$, $\theta = 65^\circ$) [14], and (c) Py ($L = 20$ nm, $M_s = 800$ emu/cc, $A_{\rm ex} = 10^{-6}$ erg/cm, $\alpha = 0.015$, $\theta = 54^\circ$) [17]. The shaded region corresponds to the bounds set by NV height range, while the dashed lines correspond to the average NV height. The experimental data in Fig. 2(a) is adapted from Ref. [13] under the CC BY 4.0 license in Nature Communications (Springer Nature), copyright 2015, Fig. 2(b) is adapted with permission from Ref. [14], AAAS, and Fig. 2(c) is adapted from Ref. [17] with permission from AIP Publishing, copyright 2020.

IV. QUANTITATIVE BENCHMARKING

We begin by benchmarking our chiral theory against recent magnon-relaxometry experiments. Specifically, we consider the hybrid of a NV center with (i) permalloy (Py) [13] [cf. Fig. 2(a)], (ii) yttrium iron garnet (YIG) [14] [cf. Fig. 2(b)], and (iii) Py, where, additionally, the NV center-thin film distance was varied [17] [cf. Fig. 2(c)]. In the first two experiments, both Γ_+ and Γ_- were measured as a function of $H_{\rm ext}$, while the third experiment measured the combined rate $\Gamma_+ + \Gamma_-$. To analyze these experiments, previous theoretical models used the achiral theory, which required arbitrary scaling factors to quantitatively fit the data [14,17]. Here, we instead apply the chiral theory (using parameters from the respective experimental references mentioned in the caption of Fig. 2) with no additional scaling factor. We highlight the influence of NV center-thin film distance via the shaded region as it was a prominent fit parameter in Refs. [13,14] in contrast to other parameters that were measured independently [41]. As the first central result of our work, we can see from Fig. 2 that the theory is in good quantitative agreement with experiments, validating the presented theoretical formalism [42].

V. CHIRAL-COUPLING-DEPENDENT RELAXATION

Having validated our theory against experiments, we next turn to understand the specific role of chirality. We begin by

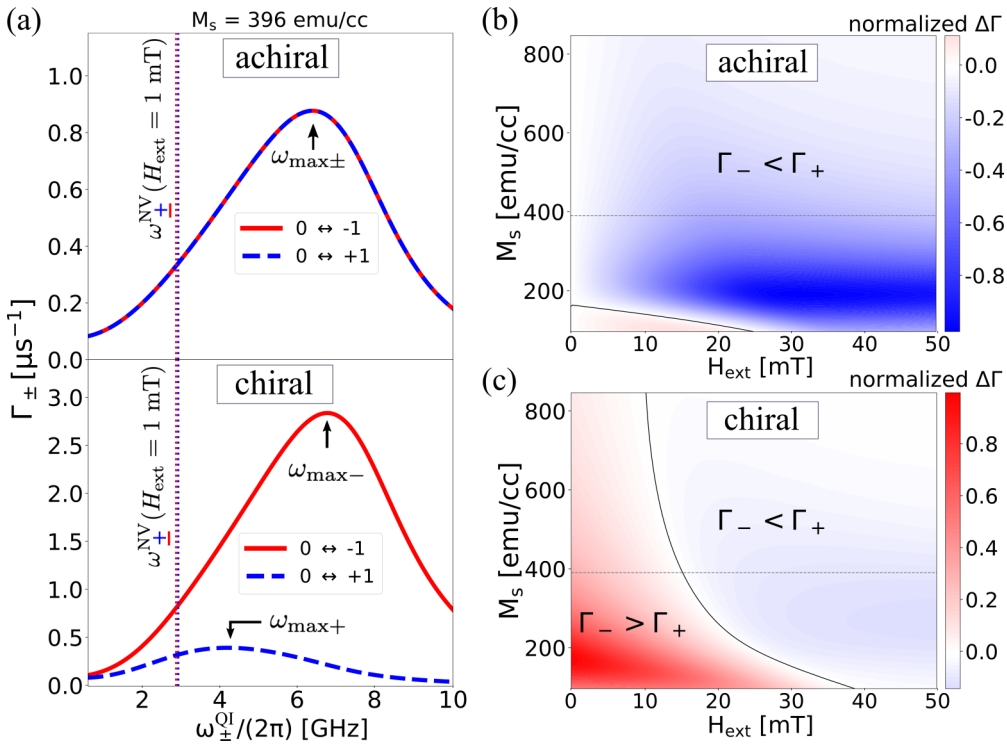

FIG. 3. (a) Computed $\Gamma_{\pm}$ as a function of $\omega_{\pm}$ for $M_s = 396$ emu/cc and $H_{ext} = 1$ mT using the achiral and chiral theory in the top and bottom panels, respectively. The vertical dotted lines mark the NV-ESR frequencies at $H_{ext} = 1$ mT. Normalized NV relaxation rate difference $\Delta\Gamma = \Gamma_- - \Gamma_+$ evaluated as a function of H_{ext} for different magnetic materials parameterized by M_s using the (b) achiral and (c) chiral theory. The parameters used are $L = 40$ nm, $\Delta/(2\pi) = 2.87$ GHz, $d_{NV} = 40$ nm, $A_{ex} = 8.47 \times 10^{-7}$ erg/cm, $\alpha = 0.05$, and $\theta_{NV} = \theta = 54.75^{\circ}$, in accordance with the relaxometry measurements presented in the next section.

plotting the relaxation rates Γ_- and Γ_+ of a hypothetical QI spin, whose transition frequencies $\omega^{QI}_{\pm}$ are scanned through the magnon spectrum. As highlighted in the Introduction, due to the chiral coupling between QI and thin film magnons, $m_s = 0 \rightarrow +1$ and $m_s = 0 \rightarrow -1$ transitions are driven by fields of unequal magnitude [cf. Figs. 1(b) and 1(c)]. Indeed, we observe that the chiral theory consequently predicts $\Gamma_- \neq \Gamma_+$ for $\omega^{QI}_- = \omega^{QI}_+$ [cf. Fig. 3(a), bottom panel]. On the other hand, the achiral theory predicts $\Gamma_- = \Gamma_+$ for $\omega^{QI}_- = \omega^{QI}_+$ [cf. Fig. 3(a), top panel].

While Fig. 3(a) highlights the key difference between the chiral and achiral theory, the relaxometry experiments are performed in the presence of an external magnetic field, which by making ω^{QI}_+ and ω^{QI}_- different, does not allow to directly measure the curve shown in Fig. 3(a). To look for an experimental signature of the chiral-coupling-induced non degenerate relaxation rates, we plot the (normalized) NV-ESR transition rate difference $\Delta\Gamma = \Gamma_- - \Gamma_+$ as a function of external field H_{ext} and for different magnetic materials (as parameterized by their saturation magnetization M_s) using the chiral and achiral theory in Figs. 3(b) and 3(c). Within both theories, for M_s below a critical value (referred to here as M^c_s, which is equal to ∼150 emu/cc for the geometrical parameters of the NV-magnet hybrid as mentioned in the caption of Fig. 3), $\Delta\Gamma$ changes signs as H_{ext} is increased. In contrast, for $M_s > M^c_s$, only Eq. (3) predicts a sign change in $\Delta\Gamma$ with H_{ext}. As explained next, the latter is an experimental signature of chiral-coupling-induced nondegenerate relaxation rates highlighted in Fig. 3(a).

To understand the relaxation rate of NV-QI, we add to Fig. 3(a) the location of NV-ESR transitions as dotted vertical lines for $H_{ext} \approx 0$. We find that M^c_s corresponds to the value of saturation magnetization above which the NVs $\omega^{NV}_{\pm}$ transitions lie below $\omega_{max\pm}$ – the frequency location that would maximize the rates $\Gamma_{\pm}$ for NV-QI within the achiral theory [43] [see Fig. 3(a), top panel]. As the field is increased, ω^{NV}_- (ω^{NV}_+) decreases (increases) linearly [see below Eq. (1)], while $\omega_{max\pm}$ shifts to a higher frequency as $\gamma\sqrt{H_{ext}(H_{ext} + H_d)}$ (as per the shift of magnon bands given by the Kittel formula [44]). Consequently, with increasing H_{ext} (for the experimentally relevant range of $H_{ext} \ll H_d$), Γ_- decreases faster than Γ_+, corresponding to ω^{NV}_- moving further below $\omega_{max\pm}$ when compared to ω^{NV}_+. $\Delta\Gamma$, therefore, decreases with increasing H_{ext} for $M_s > M^c_s$. The key point is that, since in the achiral theory $\Delta\Gamma = 0$ for $H_{ext} = 0$ [as $\omega^{NV}_+ = \omega^{NV}_-$ for $H_{ext} = 0$; cf. Fig. 3(a)–top panel], $\Delta\Gamma$ decreases from zero without a sign change as H_{ext} is increased. On the other hand, for the chiral theory, $\Delta\Gamma > 0$ for $H_{ext} = 0$, due to stronger coupling of $m_s = 0 \rightarrow -1$ to the magnon-generated fields [cf. Fig. 3(a), bottom panel], which, when combined with the decrease of $\Delta\Gamma$ with H_{ext}, imprints the predicted sign change.

VI. EXPERIMENT

To check the above picture experimentally, we present our relaxometry measurements performed on NV-nickel (Ni) thin film hybrids designed with the material and geometrical

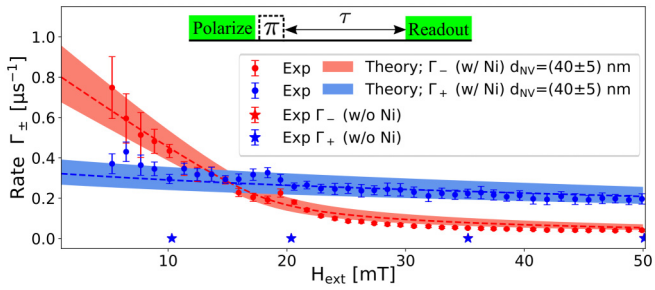

FIG. 4. Chiral coupling reflected in the relaxation rate crossover between Γ_+ and Γ_- as a function of H_{ext} in a NV-Ni thin film hybrid. Control measurements on a NV in the same diamond but in a region without the Ni film (indicated by the stars) yield NV relaxation rates below $0.003\,\mu s^{-1}$. The measurement protocol is shown in the inset. Parameters for theoretical plots are mentioned in the caption of Fig. 3.

parameters needed to observe the sign change in $\Delta\Gamma$ due to chiral coupling-induced non-degenerate relaxations [45]. We used a diamond with individually addressable NV centers implanted 10 nm below the surface, deposited a 30-nm SiO_2 spacer, and evaporated 40 nm of Ni on top. The two rates were determined by initializing the spin in each of its eigenstates (using a laser pulse and microwave pulses on the appropriate ESR transitions), waiting for a time τ that was swept, and characterizing the spin-dependent photoluminescence during a subsequent laser readout pulse (see Fig. 4 inset) [13]. Figure 4 shows a rate crossover between Γ_+ and Γ_- at $\sim$15 mT which is a clear signature that can only be captured by the presented chiral theory for evaluating the QI-spin relaxation rates [cf. Figs. 3(b) and 3(c)]. A control measurement done in absence of magnetic thin film showing rates lower by 2–3 orders of magnitude (cf. Fig. 4) confirms that thermal magnons dominate NV relaxation in the Ni-covered region.

VII. CONCLUSIONS AND OUTLOOK

In summary, we show that the magnetic-dipole transitions hosted within typical spin$>1/2$ QIs couple disparately to the chiral magnetic noise produced by thermally populated magnons in nearby magnetic films. Via presenting an experimentally benchmarked theory, we demonstrate that including this, so far neglected, role of chirality is central for quantitatively and qualitatively understanding QI-relaxometry experiments. Our results will thus assist the recently growing effort of utilizing QI relaxometry for understanding the dynamical properties of magnetic films to advance magnonics and quantum technologies utilizing magnets.

Our results can be extended to other phenomena generating chiral magnetic noise at the QI. For example, thermally populated one-way propagating magnetic modes at the boundaries of media with differing bulk band topology (as predicted by the recent theoretical proposal of topological magnon insulator [33,34]) provides a scenario where asymmetric magnon spectrum generates chiral magnetic noise. Such chiral modes also exist in electronic systems [30,31], where electrical charge fluctuations in the mode would produce the chiral magnetic noise. Combining the advantages offered by QI relaxometry (noninvasiveness, cryogenic to room temperature operation, up to nm-spatial and GHz frequency resolution) with the inherent chiral nature of QI sensors highlighted here, may thus open avenues for probing the above-mentioned phenomena of broad interest to the condensed-matter community.

ACKNOWLEDGMENTS

A.R. and P.U. acknowledge NSF DMR-1838513, NSF ECCS-1944635, and support by the U.S. Department of Energy, Office of Science through the Quantum Science Center (QSC), a National Quantum Information Science Research Center. I.B. and T.S. acknowledge support by the Dutch Research Council (NWO) through the Frontiers of Nanoscience (NanoFront) program and the Projectruimte Grant No. 680.91.115.

[1] A. V. Chumak, V. I. Vasyuchka, A. A. Serga, and B. Hillebrands, Nat. Phys. **11**, 453 (2015).
[2] Y. Li, W. Zhang, V. Tyberkevych, W.-K. Kwok, A. Hoffmann, and V. Novosad, J. Appl. Phys. **128**, 130902 (2020).
[3] D. Lachance-Quirion, Y. Tabuchi, A. Gloppe, K. Usami, and Y. Nakamura, Appl. Phys. Express **12**, 070101 (2019).
[4] P. Andrich, F. Charles, X. Liu, H. L. Bretscher, J. R. Berman, F. J. Heremans, P. F. Nealey, and D. D. Awschalom, npj Quantum Inf. **3**, 28 (2017).
[5] L. Trifunovic, F. L. Pedrocchi, and D. Loss, Phys. Rev. X **3**, 041023 (2013).
[6] J. Alicea, Rep. Prog. Phys. **75**, 076501 (2012).
[7] B. C. Stipe, H. J. Mamin, C. S. Yannoni, T. D. Stowe, T. W. Kenny, and D. Rugar, Phys. Rev. Lett. **87**, 277602 (2001).
[8] C. L. Degen, F. Reinhard, and P. Cappellaro, Rev. Mod. Phys. **89**, 035002 (2017).
[9] S. Kolkowitz, A. Safira, A. High, R. Devlin, S. Choi, Q. Unterreithmeier, D. Patterson, A. Zibrov, V. Manucharyan, H. Park *et al.*, Science **347**, 1129 (2015).
[10] A. Ariyaratne, D. Bluvstein, B. A. Myers, and A. C. B. Jayich, Nat. Commun. **9**, 2406 (2018).
[11] F. Casola, T. van der Sar, and A. Yacoby, Nat. Rev. Mater. **3**, 17088 (2018).
[12] S. Chatterjee, J. F. Rodriguez-Nieva, and E. Demler, Phys. Rev. B **99**, 104425 (2019).
[13] T. Van der Sar, F. Casola, R. Walsworth, and A. Yacoby, Nat. Commun. **6**, 7886 (2015).
[14] C. Du, T. Van der Sar, T. X. Zhou, P. Upadhyaya, F. Casola, H. Zhang, M. C. Onbasli, C. A. Ross, R. L. Walsworth, Y. Tserkovnyak *et al.*, Science **357**, 195 (2017).
[15] B. Flebus and Y. Tserkovnyak, Phys. Rev. Lett. **121**, 187204 (2018).

[16] B. Flebus, H. Ochoa, P. Upadhyaya, and Y. Tserkovnyak, Phys. Rev. B **98**, 180409(R) (2018).

[17] C. Purser, V. Bhallamudi, F. Guo, M. Page, Q. Guo, G. Fuchs, and P. Hammel, Appl. Phys. Lett. **116**, 202401 (2020).

[18] A. Finco, A. Haykal, R. Tanos, F. Fabre, S. Chouaieb, W. Akhtar, I. Robert-Philip, W. Legrand, F. Ajejas, K. Bouzehouane *et al.*, arXiv:2006.13130.

[19] E. Lee-Wong, R. Xue, F. Ye, A. Kreisel, T. van der Sar, A. Yacoby, and C. R. Du, Nano Lett. **20**, 3284 (2020).

[20] H. Zhang, M. J. H. Ku, F. Casola, C. H. R. Du, T. van der Sar, M. C. Onbasli, C. A. Ross, Y. Tserkovnyak, A. Yacoby, and R. L. Walsworth, Phys. Rev. B **102**, 024404 (2020).

[21] E. Lee-Wong, J. Ding, X. Wang, C. Liu, N. J. McLaughlin, H. Wang, M. Wu, and C. R. Du, arXiv:2009.02883.

[22] We note that the dipolar field from propagating magnons are elliptical in nature due to the finite mode ellipticity of magnons. However, in the schematic in Figs. 1(b) and 1(c), we show the dominant NV ESR transition.

[23] D. Lee, K. W. Lee, J. V. Cady, P. Ovartchaiyapong, and A. C. B. Jayich, J. Opt. **19**, 033001 (2017).

[24] D. Hopper, H. Shulevitz, and L. Bassett, Micromachines **9**, 437 (2018).

[25] H. Kraus, V. Soltamov, D. Riedel, S. Väth, F. Fuchs, A. Sperlich, P. Baranov, V. Dyakonov, and G. Astakhov, Nat. Phys. **10**, 157 (2014).

[26] T. P. M. Alegre, C. Santori, G. Medeiros-Ribeiro, and R. G. Beausoleil, Phys. Rev. B **76**, 165205 (2007).

[27] R. W. Damon and J. Eshbach, J. Phys. Chem. Solids **19**, 308 (1961).

[28] T. Yu, Y. M. Blanter, and G. E. W. Bauer, Phys. Rev. Lett. **123**, 247202 (2019).

[29] L. D. Landau, E. M. Lifšic, E. M. Lifshitz, and L. Pitaevskii, *Statistical Physics: Theory of the Condensed State* (Butterworth-Heinemann, Oxford, UK, 1980), Vol. 9; T. L. Gilbert, IEEE Trans. Magn. **40**, 3443 (2004).

[30] M. Z. Hasan and C. L. Kane, Rev. Mod. Phys. **82**, 3045 (2010).

[31] Y. Tokura, K. Yasuda, and A. Tsukazaki, Nat. Rev. Phys. **1**, 126 (2019).

[32] J. Li, Y. Li, S. Du, Z. Wang, B.-L. Gu, S.-C. Zhang, K. He, W. Duan, and Y. Xu, Sci. Adv. **5**, eaaw5685 (2019).

[33] R. Shindou, J.-i. Ohe, R. Matsumoto, S. Murakami, and E. Saitoh, Phys. Rev. B **87**, 174402 (2013).

[34] S. K. Kim and Y. Tserkovnyak, Phys. Rev. Lett. **119**, 077204 (2017).

[35] See Supplemental Material at http://link.aps.org/supplemental/10.1103/PhysRevB.102.220403 for QI relaxation rate dependence on various parameters and a detailed derivation of the theoretical expressions for evaluating the QI relaxation rates.

[36] K. Y. Guslienko and A. N. Slavin, J. Magn. Magn. Mater. **323**, 2418 (2011).

[37] Given the large demagnetization energy cost, the equilibrium magnetization typically lies in the plane of thin film, say along, say, the x axis. The magnetization deviations therefore lie in the y-z plane generating dipolar fields at the QI in the y-z plane. If the QI quantization axis is oriented along the film normal $\theta = 0^\circ$, the fluctuating dipolar field transverse to the quantization axis is linearly polarized and thus will cause equal relaxation rates for the two ESR transitions in the limit of zero external field (since linear polarization is expressible as an equal combination of the two circular polarizations).

[38] In Fourier domain, $H_{D,z} = -H_d(1 - f_k)m_z(\vec{k})$ and $H_{D,i} = -H_d f_k \sum_{j\in\{x,y\}}(k_i k_j/k^2)m_j(\vec{k})$ for $i \in \{x, y\}$ [35,36].

[39] W. F. Brown, Phys. Rev. **130**, 1677 (1963).

[40] R. Kubo and N. Hashitsume, Prog. Theor. Phys. Suppl. **46**, 210 (1970).

[41] The other material parameters also have a significant effect on the evaluated relaxation rates as shown in the Supplemental Material [35].

[42] We note that the experiments done in Ref. [13] were performed with Permalloy disk (diameter 6 micrometer) instead of an infinite thin film and this is attributed to be the source of the minor disagreement between the measurements and theory.

[43] To understand the behavior of $\Gamma_\pm$ when scanning $\omega_\pm$, we can consider the thin-film limit $kL \ll 1$, where the integrand in Eq. (3) scales as $k^2 e^{-2kd_{\rm NV}}$ with wave vector. For $\omega_\pm \approx \omega_{\rm FMR} (\equiv \omega_{sw}(\vec{k} = 0))$, the relevant wave vectors are $\vec{k} \approx 0$, for which the integrand in Eq. (3) is zero. For $\omega_\pm \gg \omega_{\rm FMR}$, large wave vectors $k \gg d_{\rm NV}^{-1}$ cause the exponential dependence to suppress the integrand and the relaxation rate is small. Thus, $\Gamma_\pm$ maximizes at some intermediate $\omega_{\rm max\pm}$.

[44] C. Kittel, Phys. Rev. **73**, 155 (1948).

[45] To ensure that experiments are done on single domain magnets, a finite external magnetic field is always applied, which can obscure the crossover between rates as in the case of NV-Py hybrids [13]. For YIG $M_s \sim 124$ emu/cc, this crossover happens at large fields where the relaxation rates are governed by the bare relaxation mechanisms. Thus, for a clear observation of this crossover signature, we propose using a ferromagnet with intermediate M_s.